Petroleum Science 23 (2026) 486–495

Contents lists available at ScienceDirect

Petroleum Science

journal homepage: www.keaipublishing.com/en/journals/petroleum-science

Original Paper

Monitoring oil pipeline microbiologically influenced corrosion (MIC) and its mitigation using a biofilm/MIC test kit

Lingjun Xu [a], Adnan Khan [b], Sarah A. Aqeel [c,*], Tingyue Gu [a,b,**]

[a] Department of Chemical & Biomolecular Engineering, Institute for Corrosion and Multiphase Technology, Ohio University, Athens, 45701, USA
[b] Department of Biological Sciences, Molecular & Cellular Biology Program, Ohio University, Athens, OH 45701, USA
[c] Aramco Research and Development Center, Saudi Aramco, Dhahran, 31311, Saudi Arabia

ARTICLE INFO

Article history:
Received 26 March 2025
Received in revised form
11 June 2025
Accepted 18 August 2025
Available online 22 August 2025

Edited by Min Li

Keywords:
MIC test kit
Biofilm test kit
MIC monitoring
Biocide efficacy
Electrochemical scan

ABSTRACT

Microbiologically influenced corrosion (MIC) is caused by microbial biofilms. In this work, an oilfield produced water sample was analyzed using a newly developed disposable electrochemical biofilm/MIC test kit consisting of two solid-state electrodes in a 10 mL standard serum vial for assessing biofilm growth, biocorrosivity and biocide treatment efficacy. The produced water sample was found to be low in microbial cell counts and nutrients. To simulate a possible worst-case scenario, the produced water sample was subcultured at 37 °C using enriched artificial seawater (EASW) for 3 rounds before being used as the seed culture for further MIC and biocide tests. The electrochemical test results from the 10 mL biofilm/MIC test kit including polarization resistance (R_p) from linear polarization resistance scans and corrosion current density (i_{corr}) from Tafel scans indicated a corrosion rate sequence of no biocide treatment > 20 ppm (*w*/*w*) tetrakis hydroxymethyl phosphonium sulfate (THPS) > 50 ppm THPS. R_p was able to predict biofilm maturity time using the incubation time when R_p leveled off (i.e., time to reach maximum corrosivity). Two common electron transfer promotors were found to accelerate MIC in the test kit vial injection tests, pointing to extracellular electron transfer-MIC as the main mechanism. This observation was consistent with the 30% corrosive sulfate reducers among all microbes in the mixed culture sample found by metagenomics. In the coupon incubation tests in 125 mL anaerobic vials, the 7-d X60 carbon steel weight loss was 1.1 ± 0.2 mg/cm^2 (2.9 mpy uniform corrosion rate) without biocide treatment. With 20 ppm THPS biocide in EASW, it dropped to 0.5 ± 0.2 mg/cm^2 (1.3 mpy), and with 50 ppm THPS, it became negligible. The corresponding MIC pit depths were 10.5, 8.9 μm, and no well-defined pits, respectively for the three biocide treatment conditions. The weight loss data confirmed the corrosion rate sequence from the biofilm/MIC test kit. This work presents a new MIC monitoring and biocide treatment assessment system for oilfield applications using the new biofilm/MIC test kit.

1. Introduction

Microbiologically influenced corrosion (MIC) is one of the major operational risks in the petroleum industry because it threatens equipment integrity by causing leaks or even catastrophic failures (Li et al., 2000; Zuo, 2007; Abdullah et al., 2014; Al-Nabulsi et al., 2015; Xu et al., 2023). Sulfate reducing bacteria (SRB) are widely distributed in some industrial systems, especially in oil and gas pipelines and reservoirs where sulfate is present in anaerobic environments due to enhanced oil recovery using seawater flooding (Barton and Fauque, 2009; Enning et al., 2012; Guan et al., 2013). SRB have been widely studied and reported to cause the most serious MIC (Javaherdashti et al., 2006; Abedi et al., 2007; Li et al., 2020).

Mechanisms of MIC have been classified into two main categories. One is extracellular electron transfer-MIC (EET-MIC) which happens when a biofilm harvests extracellular electrons from energetic metals such as elemental iron for respiration (Gu et al., 2019). In EET-MIC by an SRB biofilm, electrons released from extracellular metal oxidation are transported across cell walls to

* Corresponding author.
** Corresponding author.
E-mail addresses: sarah.aqeel.1@aramco.com (S.A. Aqeel), gu@ohio.edu (T. Gu).
Peer review under the responsibility of China University of Petroleum (Beijing).

https://doi.org/10.1016/j.petsci.2025.08.027

SRB cytoplasm for sulfate reduction under biocatalysis to produce energy (Xu et al., 2013). This behavior is explained by the biocatalytic cathodic sulfate reduction (BCSR) theory (Gu et al., 2019) using the two half reactions below,

$$\text{Extracellular}: 4Fe \rightarrow 4Fe^{2+} + 8e^{-} \ (E^{\circ} = -447\ mV_{SHE}) \quad (1)$$

$$\text{Intracellular}: SO_4^{2-} + 9H^{+} + 8e^{-} \rightarrow HS^{-} + 4H_2O \ (E^{\circ\prime} = -217\ mV_{SHE}) \quad (2)$$

in which the apostrophe in equilibrium potential $E^{\circ\prime}$ indicates physiological pH = 7 in bioelectrochemistry to replace the standard 1 M [H^+]. The coupling of the two reactions above results in a positive cell potential ($\Delta E^{\circ\prime}$) of 230 mV, which means energy is produced for SRB metabolism.

EET promoters such as riboflavin and magnetite nanoparticles (MNPs) were found to promote EET-MIC by accelerating the electron transfer process which will lead to higher MIC rates (D. Wang et al., 2022b). This means they can be used to diagnose EET-MIC. The expression level of redox-active cytochrome *c* gene in sessile nitrate reducing *Halomonas titanicae* cells was found to be increased by riboflavin, which enhanced EET capacity and MIC (Lu et al., 2024). The addition of riboflavin also promoted the growth of a key hydrogenase-positive *Desulfovibrio vulgaris* (a widely studied SRB) with H_2 as the electron donor (Ma et al., 2025). Fe^0 oxidation at neutral pH generates some molecular hydrogen at the iron surface. The hydrogenase enzymes in SRB cells can help SRB use dissolved H_2 as an electron donor for sulfate reduction (Peck, 1993; Gu et al., 2019).

$$\text{Proton reduction}: 2H^{+} + 2e^{-} \rightarrow H_2 \ (E^{\circ\prime} = -414\ mV_{SHE}) \quad (3)$$

$$H_2 \text{ oxidation}: H_2 \rightarrow 2H^{+} + 2e^{-} \quad (4)$$

Reactions (3) and (4) show that H_2 can serve as an electron carrier between SRB cells and metal surface to bridge Reaction (1) and Reaction (2), and this $2H^+/H_2$ shuttle is known to be a preferred mechanism of *D. vulgaris* MIC against Fe^0 (Woodard et al., 2023; Xu et al., 2023), which belongs to EET-MIC.

Another main MIC type is the so-called metabolite-MIC (M-MIC) in which corrosive metabolites such as organic acids secreted by acid producing bacteria (APB), and H_2S secreted by SRB with locally high concentrations underneath biofilms serve as electron acceptors (oxidants). An example is Cu MIC by SRB which uses the following reaction route,

$$2Cu + HS^{-} + H^{+} \rightarrow Cu_2S + H_2(g) \ (\Delta G^{\circ\prime} = -58.3\ kJ/mol) \quad (5)$$

The rather negative Gibbs free energy change benefits from the extremely insoluble Cu_2S, which makes H^+ a feasible electron acceptor in the corrosion of Cu despite it being a rather noble metal (Gu et al., 2019). These two different mechanisms can be distinguished by using EET promoters such as riboflavin and MNPs because M-MIC is not accelerated while EET-MIC is accelerated by them (Wang et al., 2020).

To mitigate MIC inside pipelines, biocide treatment is a primary method which targets biofilms that cause MIC (Videla, 2002; Conlette, 2014; Sharma et al., 2017; Khan et al., 2021). Treatment chemicals are usually applied during a pigging operation with a biocide plug between two pigs (Alamri, 2020; Avelino-Jiménez et al., 2023). Sessile cells in biofilms are more difficult to treat than planktonic cells because biofilms provide protections from harmful environmental conditions and antimicrobial agents (Berlanga and Guerrero, 2016; Roy et al., 2018). Tetrakis hydroxymethyl phosphonium sulfate (THPS) is one of the most popular biocides in oilfield applications due to its readily biodegradable advantage and broad-spectrum efficacy (Gao et al., 2019; Shi et al., 2023). It was found to be effective in mitigating MIC of different metals caused by SRB (Conlette, 2014; Okoro, 2015; Sharma et al., 2018; Xu et al., 2022).

In MIC studies, weight loss and pitting data are direct evidence for corrosion severity. If permitted, hanging coupons are placed inside pipelines to obtain weight loss and pitting data (Abdalsamed et al., 2020; Al-Janabi, 2020). In lab studies, electrochemical tests are also widely used as a powerful tool to support coupon weight loss results. Typical electrochemical techniques include linear polarization resistance (LPR), electrochemical impedance spectroscopy (EIS), electrochemical frequency modulation (EFM) and Tafel scans (potentiodynamic polarization scans). Many MIC studies show that properly performed electrochemical measurements generated corrosion trend results consistently in agreement with weight loss data (Badawi et al., 2010; Abdullah et al., 2014; Kalajahi et al., 2021; Yang et al., 2022; Xu et al., 2024).

In field operations, it is possible to encounter samples with low cell counts and low nutrient levels. However, biofilms can still form inside a pipeline over a long period of time (Mattila-Sandholm and Wirtanen, 1992; Schwermer et al., 2008; Liu et al., 2016). The best biofilm and MIC monitoring approach is an online sensor. However, field operators may be resistant to online sensors on existing pipelines because hole-drilling is required for installation. The only choice is to sample the pipeline fluids offline. When the nutrient levels in field samples are too low, it is possible that SRB cannot grow a biofilm on the coupons in a limited time frame under lab conditions. To facilitate lab testing, field samples are often cultured with added nutrients (Connon and Giovannoni, 2002; Lewis et al., 2021). After all, in field operations, in a less “contaminated” system, it is possible to have some locations with more robust biofilm growth as a result of more nutrients locally such as dead-legs and elbows. Solid deposits and organic nutrients (e.g., volatile fatty acids such as acetate) from crude oil may accumulate in the local water phase which promotes biofilm growth. Pipelines in some industrial systems such as oil and gas industry systems may get in contact with seawater with sufficient nutrients which can promote the growth of marine species including SRB to form a robust corrosive biofilm. Therefore, culture medium enrichment is commonly used in MIC testing of field samples (Little et al., 2006; Little and Lee, 2014).

A new disposable biofilm/MIC test kit was recently developed by our group to obtain corrosion data from electrochemical measurements that can be used to measure corrosivity and MIC type with convenience. Compared to a standard 3-electrode (3E) system consisting of a working electrode (WE), a counter electrode (CE), and dedicated reference electrode (RE) such as saturated calomel electrode (SCE), the new biofilm/MIC test kit skips the dedicated RE by using the CE as both the CE and the pseudo-RE (p-RE). This 2-electrode (2E) system avoids a fragile RE which typically involves a liquid or gel-like electrolyte and a small (glass) tube. Therefore, the setup using solid-state electrodes is more suitable for field applications at low costs, and it was confirmed that 2E scans are just as good as 3E scans in reflecting MIC rate trends (Xu et al., 2025b). The test kit can provide near real-time corrosion rate results and biocide efficacy data. It was also capable of distinguishing abiotic corrosion from biotic corrosion using Tafel skews as reported elsewhere (Xu et al., 2025a). It should be noted that for a short-term biocide kill (e.g., 0.5 h biocide solution soaking of biofilm-covered coupons) which will not generate a measurable weight loss difference due to the short exposure time, the test kit is a feasible way to provide MIC rate variations in near real-time for the biocide treatment assessment,

which can be used to corroborate sessile cell count reduction data. The test kit can be conveniently used as a first-line screening tool in the field or in labs to eliminate samples deemed low threat (showing low-corrosivity) from further costly analyses, so resources can be focused only on the most corrosive samples.

In this work, for the first time, the test kit was used for assessing an oilfield produced water sample systematically with the aim to show how the kit can be used in the field, with further analyses for confirmation. MIC mechanism was also probed using an EET promoter and metagenomics.

2. Materials and methods

2.1. Bacteria, chemicals, and metals

Oilfield microbes were grown in enriched artificial seawater (EASW) culture medium at 37 °C. The culture medium pH was adjusted to 7.0 using a 5% (*w*/*w*) NaOH solution before autoclave sterilization. EASW was then sparged with filter-sterilized N_2 gas for 1 h using a gas distributor to generate numerous tiny bubbles together with magnetic stirring to distribute the bubbles for adequate removal of dissolved oxygen. Finally, an oxygen scavenger (L-cysteine) was added to reach 20 ppm (*w*/*w*) in the culture medium in an N_2-filled anaerobic chamber.

The composition of EASW was: 3.917 g/L Na_2SO_4, 23.476 g/L NaCl, 0.192 g/L $NaHCO_3$, 0.096 g/L KBr, 0.664 g/L KCl, 0.026 g/L H_3BO_3, 0.040 g/L $SrCl_2{\cdot}6H_2O$, 10.610 g/L $MgCl_2{\cdot}6H_2O$, 1.469 g/L $CaCl_2{\cdot}2H_2O$, 1.0 g/L yeast extract, 0.5 g/L tri-sodium citrate ($Na_3C_6H_5O_7$), 3.5 g/L sodium lactate ($C_3H_5NaO_3$), 0.1 g/L $CaSO_4{\cdot}0.5H_2O$, 0.1 g/L NH_4Cl, 0.71 g/L $MgSO_4{\cdot}7H_2O$, 1.38 g/L $Fe(NH_4)_2(SO_4)_2{\cdot}6H_2O$, 0.05 g/L K_2HPO_4. Among them, yeast extract, tri-sodium citrate, sodium lactate, and $Fe(NH_4)_2(SO_4)_2{\cdot}6H_2O$ were also used as enrichment nutrients for an oilfield produced water sample which had low initial cell counts and low nutrient levels inadequate for short-term biofilm growth in the biofilm/MIC test kit vial.

X60 carbon steel for pipelines was used in this work. Table 1 shows its elemental composition. X60 coupons were polished to 600 grit finish. They were used as WEs in the biofilm/MIC test kit and also in loose coupon incubation tests in 125 mL anaerobic vials for weight loss. All the loose X60 coupons were coated with inert liquid Epoxy coating (3M Product 323) with only one working surface (1 cm^2) exposed. Isopropanol (99% by volume) was used to sanitize electrodes and coupons.

2.2. Metagenomics analysis

Metagenomics analysis was conducted by SeqCenter, LLC commercial lab in Pittsburgh, PA, USA using 16S/ITS amplicon approach (Shaffer et al., 2022). The service selected was Microbiome Sequencing: 20K 16S Reads (V3/V4 Region).

2.3. Electrochemical tests

Electrochemical tests were performed in biofilm/MIC test kit vials. Each test kit vial consisted of an X60 WE (1 cm × 1 cm working surface) and a graphite CE/p-RE in a 10 mL serum vial (Fig. 1). Each vial was sealed with a rubber septum and aluminum cap in an anaerobic chamber with two electrode wires protruding on top (Fig. 1(a)). Each liquid sample was injected into a biofilm/MIC test kit vial with a syringe needle. The excess pressure in the vial due to the 5 mL sample injection was relieved by withdrawing some headspace gas through the syringe at the end of the sampling procedure. The daily LPR measurements were performed within the range of −10 to 10 mV vs. open circuit potential (OCP) at a rate of 0.167 mV/s. Each LPR scan lasted 2 min. Tafel curves were scanned at a scan rate of 0.167 mV/s using dual-half scans (Wang et al., 2022a) from 0 to −200 mV (vs. OCP) and 0 to +200 mV (vs. OCP) in the same biofilm/MIC test kit vial. A desktop PCI4/750 potentiostat (Gamry Instruments, Warminster, PA, USA) and a CS100 portable potentiostat (Corrtest, Wuhan, China) which is suitable for field use were used in electrochemical tests.

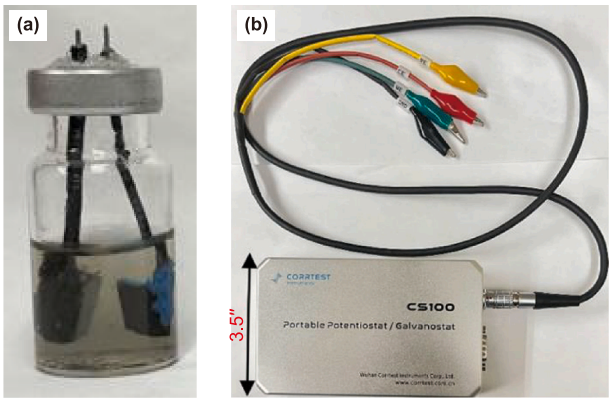

Fig. 1. **(a)** A 10 mL biofilm/MIC test kit vial consisting of an X65 WE and a graphite CE/p-RE, and **(b)** CS100 portable potentiostat (Corrtest, Wuhan, China).

Table 1
Elemental compositions (wt%) of X60 (Fe balance) (Rahman et al., 2019).

C	Mn	P	Cr	S	Si	Ni	V	Nb	Cu
0.052	1.5	0.007	0.07	0.0027	0.15	0.19	0.001	0.067	0.18

2.4. Loose coupon incubation tests in 125 mL anaerobic vials

Loose coupon incubation tests were conducted in anaerobic vials to confirm that the biofilm/MIC test kit provided the correct corrosivity trends. Three X60 coupons (1 cm^2 upward-facing working surface for each coupon) were incubated in each 125 mL anaerobic vial containing 50 mL EASW inoculated with a seed culture with a volumetric ratio of 1:100 to the culture medium. After a 7-d incubation period, coupon weight loss was measured, and sessile cell counts were enumerated. The detailed procedure for cell enumeration was documented elsewhere (Wang et al., 2020). Biofilms on the coupon surfaces were stained with the Live/Dead® BacLight™ Bacterial Viability Kit L7012 (Life Technologies, Grand Island, NY, USA) and observed under a confocal laser scanning microscope (CLSM) (Model LSM 510, Carl Zeiss, Jena, Germany). MIC pitting analysis was performed under an InfiniteFocus microscope (IFM) (Model ALC13, Alicona Imaging GmbH, Graz, Austria), which is a surface profilometer.

3. Results and discussion

3.1. Slope-shaped R_p curve from 10 mL test kit indicating biofilm growth and MIC

Fig. 2 shows polarization resistance (R_p) from the LPR curve of X65 WE incubated with a super-corrosive SRB *Desulfovibrio ferrophilus* (IS5 strain) (Wang et al., 2021) in two test kit vials. The R_p curve initially decreased (corrosion rate increased) rather than staying stable in the abiotic test (Fig. S1), suggesting biofilm build-up on the WE. The slope-shaped R_p curve reached its bottom around 3 d, which means corrosion rate peaked, suggesting

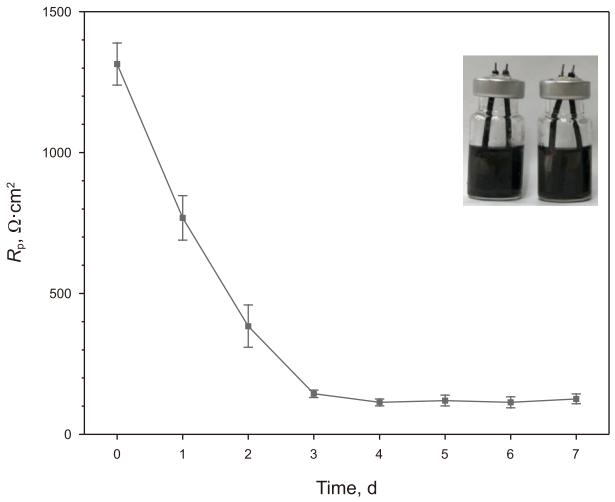

Fig. 2. R_p curve of X65 WE incubated with *D. ferrophilus* in replicate 10 mL test kit vials each containing 5 mL EASW at 37 °C for 7 d.

maturity for the biofilm on the WE inside the test kit vial. This kind of slope-shaped R_p curve is indicative of the presence of a corrosive biofilm (Xu et al., 2025b).

3.2. Test kit analysis of produced water sample with and without enrichment nutrients

This work used 1 L oilfield produced water sample (Fig. S2) collected from an entry point to the trunk line with the oil phase removed prior to putting the liquid in a bottle supplemented with 100 ppm L-cysteine oxygen scavenger. Only the water sample was analyzed because the oil phase lacked water for microbial growth and thus did not pose MIC risks.

Two biofilm/MIC test kit vials (Fig. 3), each containing 5 mL of the produced water sample, were incubated at 37 °C supplemented with newly added 100 ppm L-cysteine (vial a), and the aforementioned enrichment nutrients plus 100 ppm L-cysteine (vial b). Because 100 ppm L-cysteine was previously added already during sample collection in the field, each vial at this time had 200 ppm L-cysteine cumulatively. The top brownish oily matter, which was found to possess an oil smell, in the biofilm/MIC test kit vial with L-cysteine addition only (vial a) was found to be residual oil separated from the water phase with the help of the small amount ferrous ions from $Fe(NH_4)_2(SO_4)_2{\cdot}6H_2O$ introduced by the enrichment nutrients, and released from the low-level water corrosion of X60 at pH = 7 (Almojjly et al., 2018; Wang et al., 2020). Additional information about the oil separation phenomenon is included in the Supplemental Information (Fig. S3). The color was not from iron oxides as the result of oxygen leak. It appeared even without any coupons in the vial (Fig. S3).

Fig. 3(c) shows that after a 7-d incubation, nutrient enrichment led to healthy SRB growth as indicated by the dark black broth color, characteristic of SRB growth with FeS precipitation (Zhou et al., 2014), while in the absence of the enrichment nutrients, the culture medium did not yield any black color, and the broth was not that turbid. The vials with black color were found to contain H_2S judging from the headspace gas detection using a H_2S detector, and the distinct rotten egg smell when the vials were opened. The R_p curves in Fig. 4(a) confirmed that the slope-shaped MIC trend only existed in the enriched growth test kit vial. Thus, the as-received oilfield produced water sample was not suitable for direct analysis due to low cell counts and low nutrients, which could not grow a detectable biofilm in 7 d. In such a case, a common case is to enrich the culture medium (Guasch et al., 1995; Hageskal et al., 2022). At 5 d during the 7-d of incubation, the slope-shaped R_p curve for the enriched growth vial started to level off. At 7 d, riboflavin injection and THPS biocide injection were conducted in tandem. In Fig. 4(b), the two injections resulted in 17% R_p decrease and 21% R_p increase, respectively. The injection test results confirmed EET-MIC as the main MIC mechanism in the enriched growth based on EET promotor increasing corrosivity, and the biofilm kill effect of 100 ppm (*w*/*w*) THPS which decreased corrosivity.

3.3. Test kit testing of third subculture of the produced water sample

Fig. 4(a) suggests that the field produced water sample was incapable of growing a corrosive biofilm without enrichment. However, a field system may be different from the static lab setting because a corrosive biofilm can grow in certain locations such as dead legs and elbows in a pipeline where water and nutrients tend to accumulate. Given sufficient time, biofilms can grow and maintain their health by extracting nutrients from the

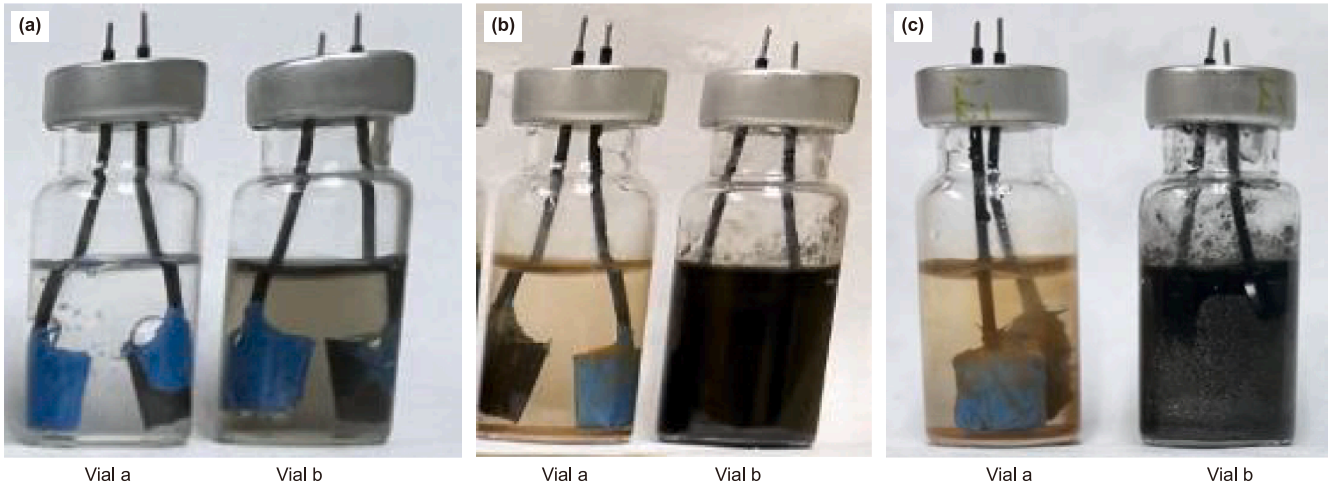

Fig. 3. 10-mL test kit vials containing 5 mL produced water sample with (Vial a) 100 ppm L-cysteine added during field sample collection, and (Vial b) with additional enrichment nutrients and 100 ppm L-cysteine at different incubation times: **(a)** 0 d, **(b)** 5 d, and **(c)** 7 d at 37 °C.

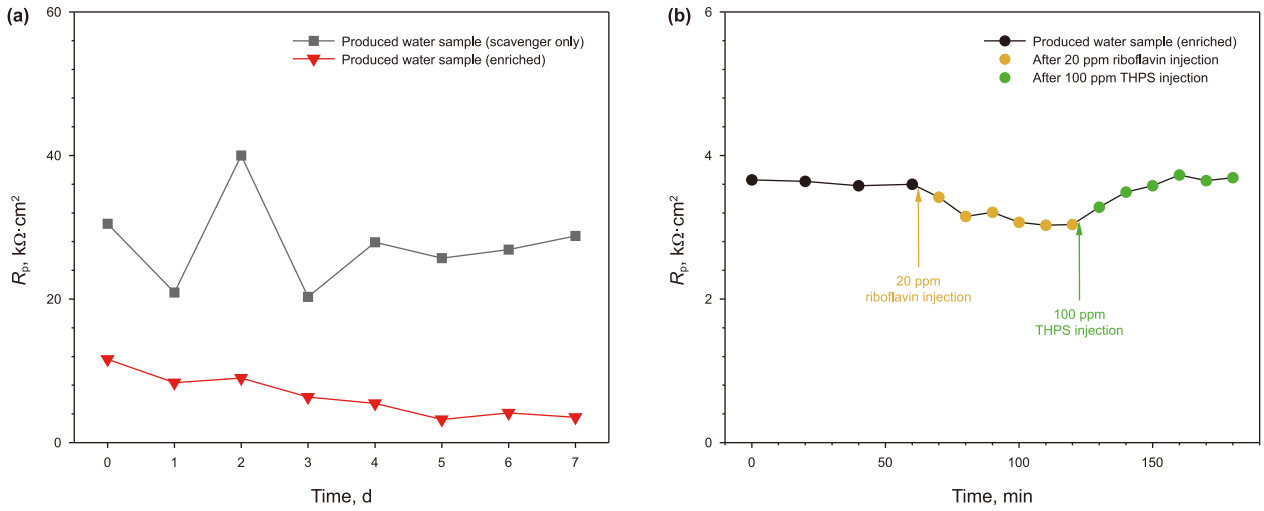

Fig. 4. **(a)** R_p curves of X60 WEs in two 10 mL test kit vials injected with the produced water sample with and without nutrient enrichment during 7-d incubation at 37 °C, and **(b)** R_p response of X60 WE in the 10 mL biofilm test kit vial subjected to tandem injections of riboflavin (electron mediator) and THPS biocide.

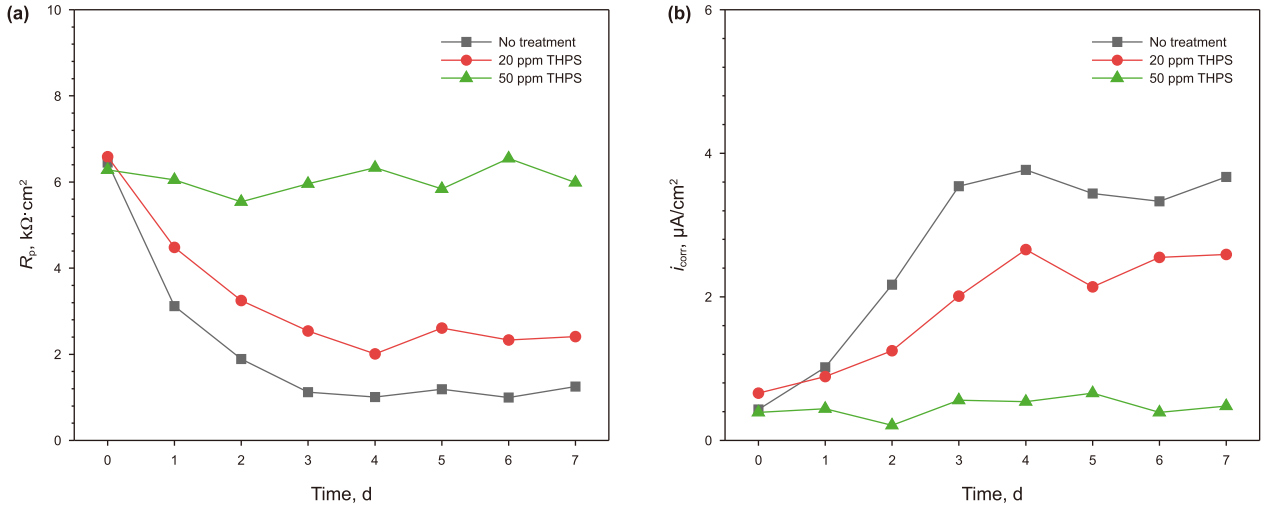

Fig. 5. R_p curves from LPR **(a)**, and i_{corr} curves from Tafel **(b)** of X60 WEs during 7-d incubation in biofilm test kit vials containing 5 mL EASW inoculated with third subculture of the produced water sample at 37 °C.

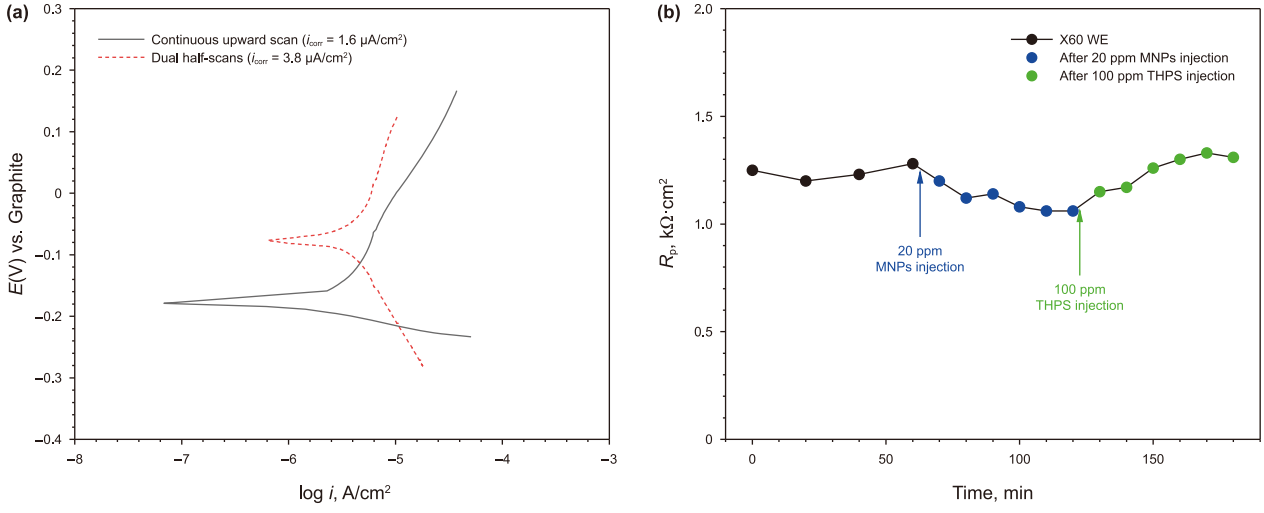

Fig. 6. **(a)** Tafel skews in the Tafel curves of X60 WE from continuous upward scan (from bottom to top) compared to milder dual-half scans (with both half scans starting from OCP), and **(b)** R_p response of X60 WE tandem injections of EET-promoting MNPs and THPS in 10 mL biofilm/MIC test kit vial containing 5 mL EASW inoculated with third subculture of the produced water sample at 37 °C at 3 d.

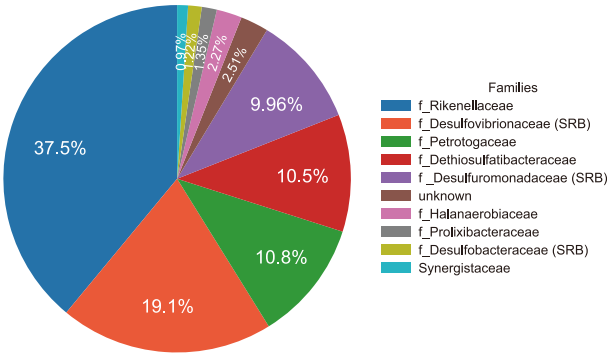

Fig. 7. Composition of major bacterial families in the third subculture of the produced water sample based on a metagenomics analysis.

pipeline fluid (Hall-Stoodley et al., 2004; Xu et al., 2019; Stoodley et al., 1994). To simulate a possible worst-case scenario in the field, the produced water sample (Fig. S2) was subcultured to promote the growth of corrosive SRB in 125 mL anaerobic vials with 50 mL EASW. This subculture procedure was repeated two more times. The third subculture was then used as the seed culture for biocide treatment testing in the 10 mL biofilm/MIC test kit vials (Fig. S4). After a 7-d incubation, the samples with no treatment and 20 ppm THPS showed SRB growth indicated by the black color (Fig. S4). With 50 ppm THPS, no obvious SRB growth was visible, suggesting that 50 ppm THPS was effective in preventing SRB growth. In a previous biocide study in the lab, it was found that 20 ppm THPS was only slightly effective in preventing *D. ferrophilus* biofilm growth, but 50 ppm was sufficient in completely inhibiting MIC by *D. ferrophilus* in EASW (J. Wang et al., 2022).

The R_p curves in Fig. 5(a) show that without biocide treatment, a typical slope-shaped MIC trend is shown, indicating a biofilm maturity time of 3 d. With 20 ppm THPS, the R_p curve was higher (reflecting lower corrosion) compared to no treatment with biofilm matured at 4 d. Based on the reduction in the level-off R_p value, the 20 ppm THPS MIC inhibition efficiency was 58%. The 50 ppm THPS curve does not exhibit an obvious decreasing R_p trend in Fig. 5(a), suggesting excellent MIC inhibition. Thus, the corrosion rate sequence is no treatment >20 ppm THPS >50 ppm THPS. The corrosion current density (i_{corr}) curves in Fig. 5(b) also suggest the same sequence. The MIC inhibition efficiency based on i_{corr} reduction is 43% for 20 ppm THPS which is not far from 58% based on R_p data in Fig. 5(a).

Usually, R_p curves are preferred because LPR scans are much faster (2 min in this work) and less harsh voltage (±10 mV vs. OCP compared to ±200 mV vs. OCP) toward the biofilms on WEs than Tafel scans (60 min in this work). However, i_{corr} curves are useful for clarification when R_p trend is ambiguous. For Tafel scans, dual-half scans must be used instead of harsh continuous upward scan because the later can alter the WE surface according to a previous study (Wang et al., 2022a).

Fig. 6(a) shows Tafel curves of X60 WE at 3 d of incubation in 5 mL EASW inoculated with the third subculture of the produced water sample. Compared to the dual-half scan curve, the Tafel curve obtained from a continuous upward scan (from −200 mV vs. OCP to +200 mV vs. OCP) exhibited large distortions in Tafel curve shapes including compression in the cathodic curve and elongation in the anodic curve. The corrosion potentials (E_{corr}) also shifted considerably, and a large i_{corr} decrease (58%) was observed for the continuous upward scan. This "Tafel skew" phenomenon was because the continuous upward scan applied the extreme external voltage (−200 mV vs. OCP) without allowing any time for the biofilm on the WEs to adapt to it (D. Wang et al., 2022a). This has been recently found to be an effective approach to

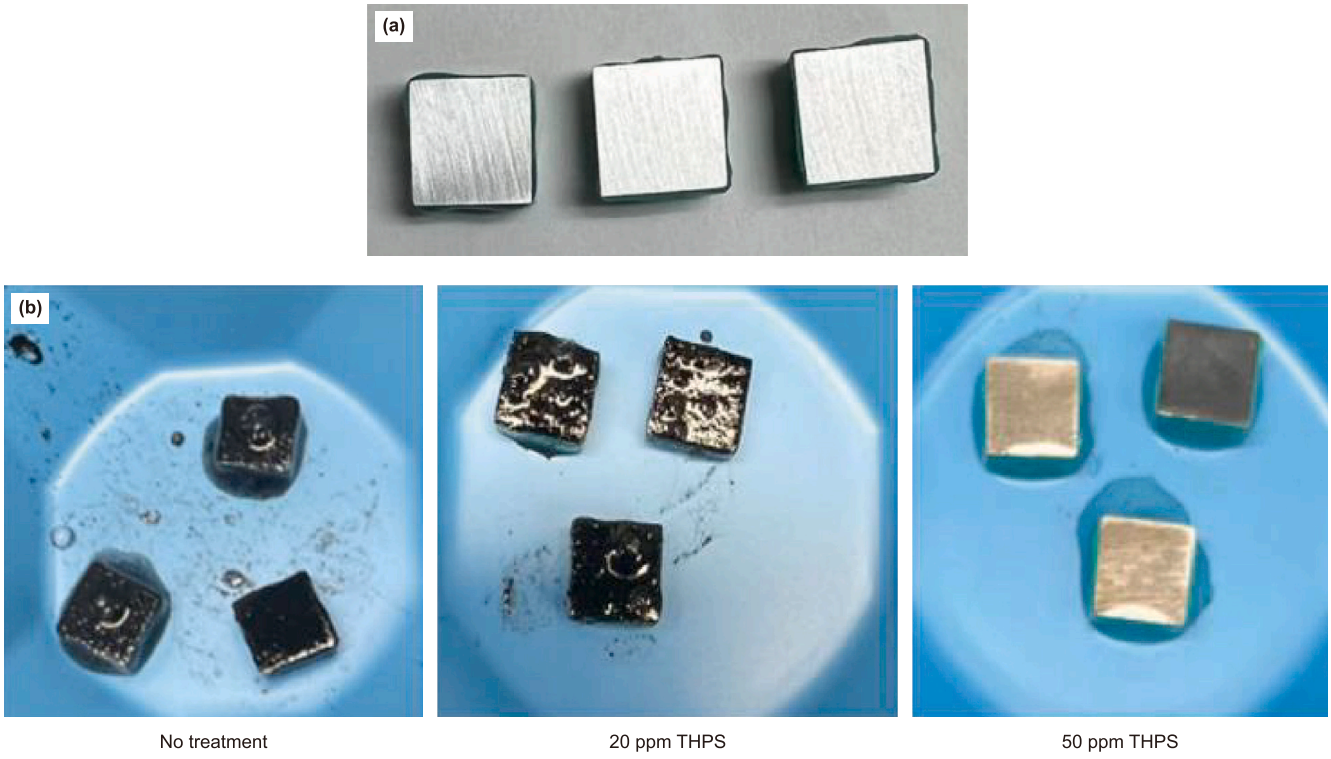

Fig. 8. X60 coupons (1 cm^2) before **(a)** and after **(b)** 7-d incubation in EASW inoculated with third subculture of the produced water sample.

distinguishing MIC from abiotic corrosion (Xu et al., 2025a). Therefore, Tafel scan results in the biofilm/MIC test kit confirmed the existence of MIC on WE caused by the third subculture of the produced water sample. Thus, the test kit can be conveniently used with a portable potentiostat in the field to identify MIC.

The 20 ppm MNPs injection into the test kit vial at 3 d of incubation resulted in a 15% R_p decrease within 1 h (Fig. 6(b)), indicating that EET-MIC against X60 carbon steel was accelerated by this EET promoter, which had a similar effect as riboflavin as shown in Fig. 4(b). The subsequent 100 ppm THPS injection caused 24% R_p increase, again manifesting the effectiveness of THPS in mitigating SRB MIC.

3.4. Metagenomics analysis

Metagenomics analysis of the third subculture of the produced water sample is shown in Fig. 7. The result using the 16S/ITS amplicon approach revealed a broad range of bacterial species including sulfate reducers, which accounted for 30% of the total microbial population. The most dominant family was found to be Rikenellaceae which accounted for 37% of the total microbial population. However, the corrosivity of Rikenellaceae bacteria was not documented in literature. SRB biofilms are "bottom-feeders" that harvest extracellular electrons from carbon steels (Gu et al., 2015). Only those sessile cells in one or a few layers on the metal surface are capable of EET while the sessile cells above them may share the energy without direct involvement in EET-MIC (Gu et al., 2019). Thus, in mixed-culture MIC, SRB cells do not need to dominate the microbial population to cause significant MIC. In this work, 30% SRB can sufficiently account for MIC in this work.

3.5. Loose coupon incubation with and without biocide treatment using subculture as seed in 125 mL anaerobic vials

Loose coupon incubation tests were conducted in 125 anaerobic vials (Fig. S5) to confirm the corrosion rate sequence results from the biofilm/MIC test kit and to provide additional sessile cell count and biofilm image data. Each 125 mL vial with 50 mL EASW was inoculated with 0.5 mL seed culture (the third subculture of the produced water sample). After the 7-d incubation, SRB growth was seen in the anaerobic vials with no treatment and with 20 ppm THPS, but no black color (i.e., negligible SRB growth) was observed with 50 ppm THPS, which was consistent with the 10 mL biofilm/MIC test kit results (Fig. S4).

The coupon images before and after the 7-d incubation are presented in Fig. 8. Black sludge common in SRB MIC carbon steel (Javed et al., 2017) was observed on coupons with no treatment and 20 ppm THPS treatment. With 50 ppm THPS, no obvious black color is observed in Fig. 8. The loose sludge was rinsed off before

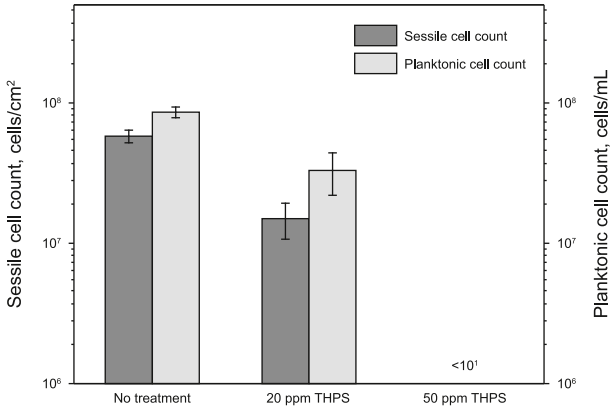

Fig. 9. Planktonic cell counts and sessile cell counts on X60 coupons after 7-d incubation in EASW inoculated with third subculture of the produced water sample at 37 °C.

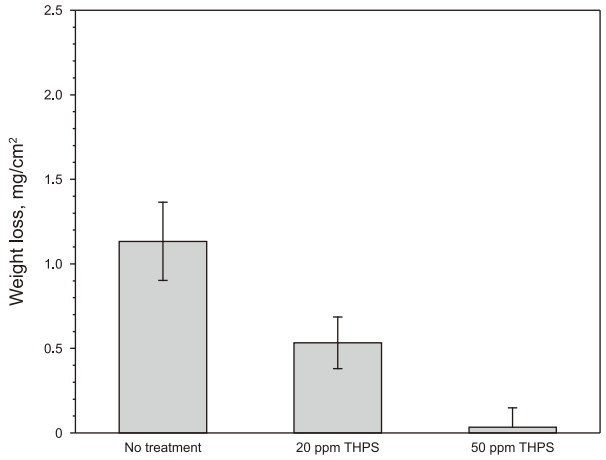

Fig. 11. Weight losses of X60 coupons after 7-d incubation in 125 mL vials containing 50 mL EASW inoculated with third subculture of the produced water sample.

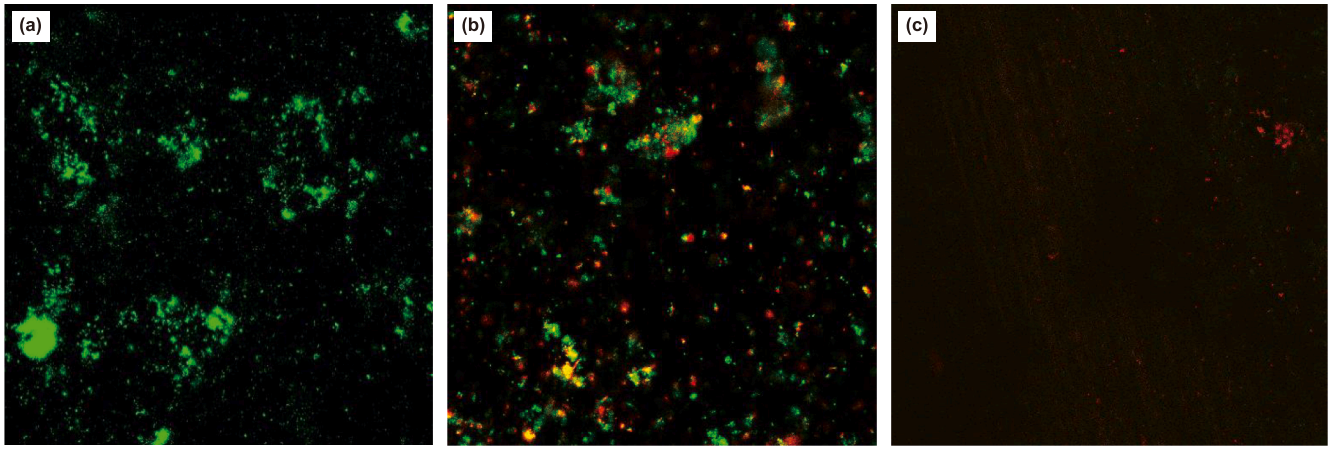

Fig. 10. CLSM images of biofilms on X60 coupons after 7-d incubation in 125 mL vials containing 50 mL EASW inoculated with third subculture of the produced water sample at 37 °C with **(a)** no biocide treatment, **(b)** 20 ppm THPS, and **(c)** 50 ppm THPS.

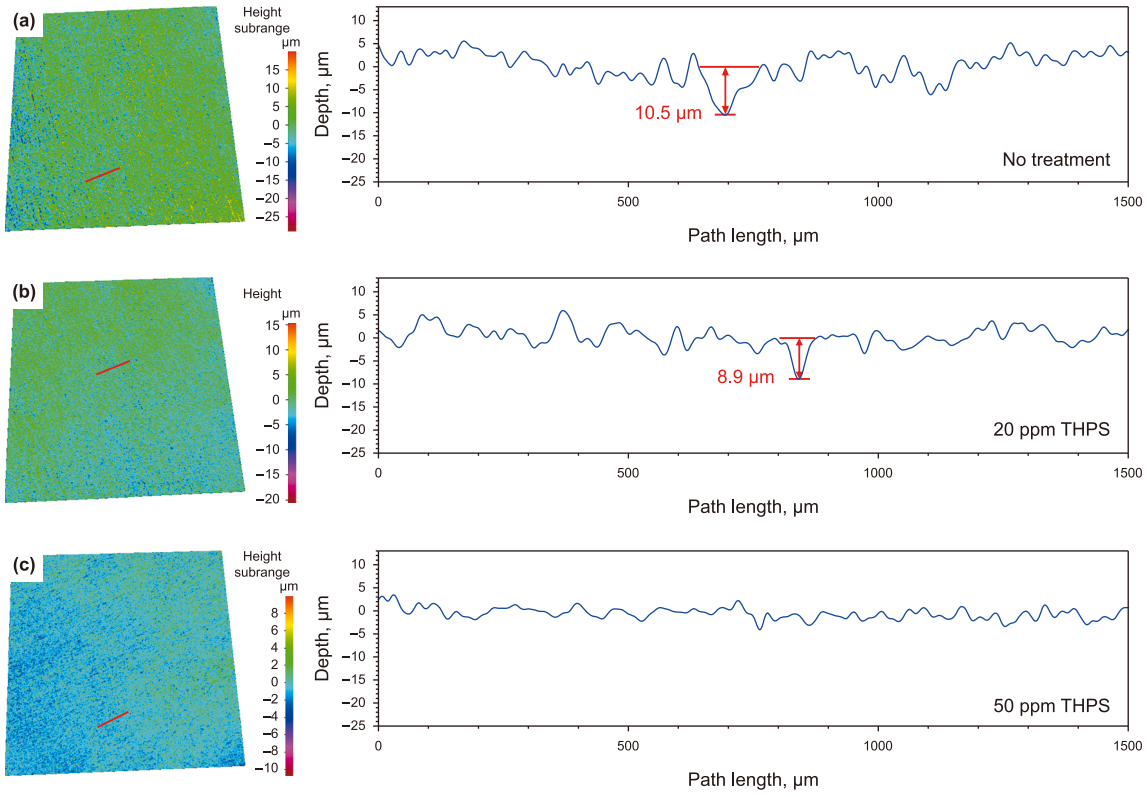

Fig. 12. IFM pit images and surface profiles across the deepest pits on X60 coupons after 7-d incubation in 125 mL vials containing 50 mL EASW inoculated with third subculture of the produced water sample with **(a)** no treatment, **(b)** 20 ppm THPS, and **(c)** 50 ppm THPS at 37 °C.

cell counting and CLSM imaging. Fig. 9 shows that 20 ppm THPS achieved 0.6-log and 0.4-log reductions in sessile cells and planktonic cells, respectively (no treatment vs. 20 ppm THPS, *p*-value <0.05 for both sessile and planktonic cell counts), while 50 ppm THPS achieved at least 6.7-log and 6.9-log reductions, respectively (20 ppm THPS vs. 50 ppm THPS, *p*-value <0.05). Using a commercial SRB test kit (Biosan Lab Inc., USA), the SRB sessile cell counts were found to be 10^7–10^8, 10^6–10^7, and $<10^1$ cells/cm^2 for the coupons with no treatment, 20 ppm THPS, and 50 ppm THPS, respectively. The SRB sessile cell readings and reductions were similar to the hemocytometer cell count results, except the third cell count which was below the threshold for detection by a hemocytometer. Motile SRB cells were easily distinguished from FeS particles under a 400X microscope.

The CLSM biofilm image in Fig. 10(a) suggests healthy biofilm formation on the X60 coupon in the absence of THPS with abundant live cells (green dots) and no dead cells (red dots) present. With 20 ppm THPS, there were still plenty of live cells in the biofilm, but dead cells also appeared in Fig. 10(b) which indicated marginal biocide kill effect by 20 ppm THPS. With 50 ppm THPS, live cells were hardly seen with some dead cells still remained in the biofilm in Fig. 10(c) after they were killed. The CLSM results here are consistent with the sessile cell counts in Fig. 9.

After the 7-d incubation, the weight losses of X60 coupons with no treatment, 20 ppm THPS, and 50 ppm THPS were 1.1 ± 0.2 mg/cm^2 (2.9 mpy uniform corrosion rate), 0.5 ± 0.2 mg/cm^2 (1.3 mpy) (no treatment vs. 20 ppm THPS, *p*-value <0.05), and 0.03 ± 0.11 mg/cm^2 (0.08 mpy) (20 ppm THPS vs. 50 ppm THPS, *p*-value <0.05), respectively in Fig. 11. The 20 ppm THPS in the culture medium reduced weight loss by 53%, and 50 ppm THPS made weight loss negligible. The results proved that 50 ppm THPS was sufficient in preventing MIC in this work. Here, the weight loss data are consistent with the sessile cell count trend in Fig. 9.

The pitting data in Fig. 12 reveal that without THPS, a maximum pit depth of 10.5 μm was observed on the X60 coupons after the 7-d incubation in EASW inoculated with the third subculture of the produced water sample. With 20 ppm THPS in EASW, the maximum pit depth was reduced to 8.9 μm. With 50 ppm THPS, no well-defined MIC pits were found in Fig. 12. Therefore, the coupon incubation test results corroborated electrochemical test results above, just like in other MIC studies using coupon tests and full-size electrochemical glass cells with three electrodes in literature (Wang et al., 2020; Pu et al., 2023; Xu et al., 2025b).

4. Conclusion

This work demonstrated a systematic approach using a disposable electrochemical biofilm/MIC test kit in analyzing oilfield samples with low microbial cell counts and nutrients, which necessitated subculturing with enrichment nutrients. Biocide mitigation was also assessed using the test kit. The biofilm/MIC test kit was found to provide biocorrosivity and biocide efficacy trends adequately, and they matched traditional sessile cell count, weight loss and pit depth data trends from coupon incubation in 125 mL anaerobic vials. The test kit provided additional transient insights. The kit was able to assess biocide efficacies for both biofilm prevention (biocide added before incubation) and biofilm kill (biocide injected after biofilm maturity). Tafel skews and injection of EET promoters helped to confirm MIC and its EET-MIC mechanism. Furthermore, metagenomics data supported EET-MIC mechanism.

CRediT authorship contribution statement

Lingjun Xu: Writing – original draft, Visualization, Validation, Investigation, Formal analysis, Data curation. **Adnan Khan:** Validation, Investigation, Formal analysis, Data curation. **Sarah A. Aqeel:** Supervision, Resources. **Tingyue Gu:** Writing – review & editing, Supervision, Resources, Project administration, Methodology, Funding acquisition, Conceptualization.

Declaration of competing interest

The authors declare that they have no known competing financial interests or personal relationships that could have appeared to influence the work reported in this paper.

Acknowledgements

This work was financially supported by Saudi Aramco. Some results in this work were presented in the AMPP Annual Conference + Expo in April 2025 (Paper No. C2025-00286).

Supplementary data

Supplementary data to this article can be found online at https://doi.org/10.1016/j.petsci.2025.08.027.

References

Abdalsamed, I.A., Amar, I.A., Altohami, F.A., Salih, F., Mazek, M., Ali, M., Sharif, A., 2020. Corrosion strategy in oil field system. J. Chem. Rev. 2, 28–39. https://doi.org/10.33945/SAMI/JCR.2020.1.2.

Abdullah, A., Yahaya, N., Md Noor, N., Mohd Rasol, R., 2014. Microbial corrosion of API 5L X-70 carbon steel by ATCC 7757 and consortium of sulfate-reducing bacteria. J. Chem. 2014. https://doi.org/10.1155/2014/130345.

Abedi, S.Sh, Abdolmaleki, A., Adibi, N., 2007. Failure analysis of SCC and SRB induced cracking of a transmission oil products pipeline. Eng. Fail. Anal. 14, 250–261. https://doi.org/10.1016/j.engfailanal.2005.07.024.

Alamri, A.H., 2020. Localized corrosion and mitigation approach of steel materials used in oil and gas pipelines–An overview. Eng. Fail. Anal. 116, 104735. https://doi.org/10.1016/j.engfailanal.2020.104735.

Al-Janabi, Y.T., 2020. An overview of corrosion in oil and gas industry: upstream, midstream, and downstream sectors. Corros. Inhib. Oil Gas Indust. 1–39. https://doi.org/10.1002/9783527822140.ch1.

Almojjly, A., Johnson, D., Oatley-Radcliffe, D.L., Hilal, N., 2018. Removal of oil from oil-water emulsion by hybrid coagulation/sand filter as pre-treatment. J. Water Process Eng. 26, 17–27. https://doi.org/10.1016/j.jwpe.2018.09.004.

Al-Nabulsi, K.M., Al-Abbas, F.M., Rizk, T.Y., Salameh, A.E.M., 2015. Microbiologically assisted stress corrosion cracking in the presence of nitrate reducing bacteria. Eng. Fail. Anal. 58, 165–172. https://doi.org/10.1016/j.engfailanal.2015.08.003.

Avelino-Jiménez, I., Hernández-Maya, L., Larios-Serrato, V., Quej-Ake, L., Castelán-Sánchez, H., Herrera-Díaz, J., Garibay-Febles, V., Rivera-Olvera, J., Zavala-Olivares, G., Zapata-Peñasco, I., 2023. Biofouling and biocorrosion by microbiota from a marine oil pipeline: a metagenomic and proteomic approach. J. Environ. Chem. Eng. 11, 109413. https://doi.org/10.1016/j.jece.2023.109413.

Badawi, A., Hegazy, M., El-Sawy, A., Ahmed, H., Kamel, W., 2010. Novel Quaternary ammonium hydroxide cationic surfactants as corrosion inhibitors for carbon steel and as biocides for sulfate reducing bacteria (SRB). Mater. Chem. Phys. 124, 458–465. https://doi.org/10.1016/j.matchemphys.2010.06.066.

Barton, L.L., Fauque, G.D., 2009. Biochemistry, physiology and biotechnology of sulfate-reducing bacteria. Adv. Appl. Microbiol. 68, 41–98. https://doi.org/10.1016/S0065-2164(09)01202-7.

Berlanga, M., Guerrero, R., 2016. Living together in biofilms: the microbial cell factory and its biotechnological implications. Microb. Cell Fact. 15, 1–11. https://doi.org/10.1186/s12934-016-0569-5.

Conlette, O., 2014. Impacts of Tetrakis-hydroxymethyl phosphonium sulfate (THPS) based biocides on the functional group activities of Some oil field microorganisms associated with corrosion and souring. BMRJ 4, 1463–1475. https://doi.org/10.9734/BMRJ/2014/11943.

Connon, S.A., Giovannoni, S.J., 2002. High-throughput methods for culturing microorganisms in very-low-nutrient media yield diverse new marine isolates. Appl. Environ. Microbiol. 68, 3878–3885. https://doi.org/10.1128/AEM.68.8.3878-3885.2002.

Enning, D., Venzlaff, H., Garrelfs, J., Dinh, H.T., Meyer, V., Mayrhofer, K., Hassel, A.W., Stratmann, M., Widdel, F., 2012. Marine sulfate-reducing bacteria cause serious corrosion of iron under electroconductive biogenic mineral crust. Environ. Microbiol. 14, 1772–1787. https://doi.org/10.1111/j.1462-2920.2012.02778.x.

Gao, D., Wang, P., Shi, J., Li, F., Li, W., Lyu, B., Ma, J., 2019. A green chemistry approach to leather tanning process: cage-like octa (aminosilsesquioxane) combined with Tetrakis (hydroxymethyl) phosphonium sulfate. J. Clean. Prod. 229, 1102–1111. https://doi.org/10.1016/j.jclepro.2019.05.008.

Gu, T., Jia, R., Unsal, T., Xu, D., 2019. Toward a better understanding of microbiologically influenced corrosion caused by sulfate reducing bacteria. J. Mater. Sci. Technol. 35, 631–636. https://doi.org/10.1016/j.jmst.2018.10.026.

Gu, T., Xu, D., Zhang, P., Li, Y., Lindenberger, A.L., 2015. Microbiologically influenced corrosion and its impact on metals and other materials. Microbiol. Min. Metals Mater. Environ. 25, 383–408. https://doi.org/10.1201/b18124-15.

Guan, J., Xia, L.P., Wang, L.Y., Liu, J.F., Gu, J.D., Mu, B.Z., 2013. Diversity and distribution of sulfate-reducing bacteria in four petroleum reservoirs detected by using 16S rRNA and dsrAB genes. Int. Biodeterior. Biodegrad. 76, 58–66. https://doi.org/10.1016/j.ibiod.2012.06.021.

Guasch, H., Martí, E., Sabater, S., 1995. Nutrient enrichment effects on biofilm metabolism in a Mediterranean stream. Freshw. Biol. 33, 373–383. https://doi.org/10.1111/j.1365-2427.1995.tb00399.x.

Hageskal, G., Heggeset, T.M.B., Nguyen, G.-S., Haugen, T., Jønsson, M., Egas, C., Hidalgo, A., Wentzel, A., Lewin, A.S., 2022. Flow-based method for biofilm microbiota enrichment and exploration of metagenomes. AMB Express 12, 36. https://doi.org/10.1186/s13568-022-01377-y.

Hall-Stoodley, L., Costerton, J.W., Stoodley, P., 2004. Bacterial biofilms: from the Natural environment to infectious diseases. Nat. Rev. Microbiol. 2, 95–108. https://doi.org/10.1038/nrmicro821.

Javaherdashti, R., Raman, R.S., Panter, C., Pereloma, E.V., 2006. Microbiologically assisted stress corrosion cracking of carbon steel in mixed and pure cultures of sulfate reducing bacteria. Int. Biodeterior. Biodegrad. 58, 27–35. https://doi.org/10.1016/j.ibiod.2006.04.004.

Javed, M., Neil, W., McAdam, G., Wade, S., 2017. Effect of sulphate-reducing bacteria on the microbiologically influenced corrosion of ten different metals using constant test conditions. Int. Biodeterior. Biodegrad. 125, 73–85. https://doi.org/10.1016/j.ibiod.2017.08.011.

Kalajahi, S.T., Rasekh, B., Yazdian, F., Neshati, J., Taghavi, L., 2021. Corrosion behaviour of X60 steel in the presence of sulphate-reducing bacteria (SRB) and iron-reducing bacteria (IRB) in seawater. Corrosion Eng. Sci. Technol. 56, 543–552. https://doi.org/10.1080/1478422X.2021.1919840.

Khan, M., Hussain, M., Djavanroodi, F., 2021. Microbiologically influenced corrosion in oil and gas industries: a review. Int. J. Corros. Scale Inhib. 10, 80–106. https://doi.org/10.17675/2305-6894-2021-10-1-5.

Lewis, W.H., Tahon, G., Geesink, P., Sousa, D.Z., Ettema, T.J., 2021. Innovations to culturing the uncultured microbial majority. Nat. Rev. Microbiol. 19, 225–240. https://doi.org/10.1038/s41579-020-00458-8.

Li, S.Y., Kim, Y.G., Jeon, K.S., Kho, Y.T., 2000. Microbiologically influenced corrosion of underground pipelines under the disbonded coatings. Met. Mater. 6, 281–286. https://doi.org/10.1007/BF03028224.

Li, Y., Feng, S., Liu, H., Tian, X., Xia, Y., Li, M., Xu, K., Yu, H., Liu, Q., Chen, C., 2020. Bacterial distribution in SRB biofilm affects MIC pitting of carbon steel studied using FIB-SEM. Corros. Sci. 167, 108512. https://doi.org/10.1016/j.corsci.2020.108512.

Little, B., Lee, J.S., Ray, R., 2006. Diagnosing microbiologically influenced corrosion: a state-of-the-art review. Corrosion 62, 1006–1017. https://doi.org/10.5006/1.3278228.

Little, B.J., Lee, J.S., 2014. Microbiologically influenced corrosion: an update. Int. Mater. Rev. 59, 384–393. https://doi.org/10.1179/1743280414Y.0000000035.

Liu, S., Gunawan, C., Barraud, N., Rice, S.A., Harry, E.J., Amal, R., 2016. Understanding, monitoring, and controlling biofilm growth in drinking water distribution systems. Environ. Sci. Technol. 50, 8954–8976. https://doi.org/10.1021/acs.est.6b00835.

Lu, S., Zhang, L., Xue, N., Chen, S., Xia, M., Fu, M., Gao, Y., Dou, W., 2024. Riboflavin-mediated Fe0-to-microbe electron transfer corrosion of EH40 steel by *Halomonas titanicae*. Corros. Sci. 231, 111981. https://doi.org/10.1016/j.corsci.2024.111981.

Ma, P., Wang, D., Xu, D., Lovley, D.R., 2025. Evaluating the importance of Flavin-Based electron shuttling in corrosion. Corros. Sci., 112782 https://doi.org/10.1016/j.corsci.2025.112782.

Mattila-Sandholm, T., Wirtanen, G., 1992. Biofilm formation in the industry: A review. Food Rev. Int. 8, 573–603. https://doi.org/10.1080/87559129209540953.

Okoro, C.C., 2015. The biocidal efficacy of Tetrakis-hydroxymethyl phosphonium sulfate (THPS) based biocides on oil pipeline PigRuns liquid biofilms. Petrol. Sci. Technol. 33, 1366–1372. https://doi.org/10.1080/10916466.2015.1062781.

Peck, H.D., 1993. Bioenergetic strategies of the sulfate-reducing bacteria. In: Odom, J.M., Singleton, R. (Eds.), The Sulfate-Reducing Bacteria: Contemporary Perspectives, Brock/Springer Series in Contemporary Bioscience. Springer New York, New York, NY, pp. 41–76. https://doi.org/10.1007/978-1-4613-9263-7_3.

Pu, Y., Tian, Y., Hou, S., Dou, W., Chen, S., 2023. Enhancement of exogenous riboflavin on microbiologically influenced corrosion of nickel by electroactive *Desulfovibrio vulgaris* biofilm. npj Mater. Degrad. 7, 7. https://doi.org/10.1038/s41529-023-00325-w.

Rahman, K.M., Mohtadi-Bonab, M.A., Ouellet, R., Szpunar, J., 2019. A comparative study of the role of hydrogen on degradation of the mechanical properties of API X60, X60SS, and X70 pipeline steels. Steel Res. Int. 90, 1900078. https://doi.org/10.1002/srin.201900078.

Roy, R., Tiwari, M., Donelli, G., Tiwari, V., 2018. Strategies for combating bacterial biofilms: a focus on anti-biofilm agents and their mechanisms of action. Virulence 9, 522–554. https://doi.org/10.1080/21505594.2017.1313372.

Schwermer, C.U., Lavik, G., Abed, R.M., Dunsmore, B., Ferdelman, T.G., Stoodley, P., Gieseke, A., De Beer, D., 2008. Impact of nitrate on the structure and function of bacterial biofilm communities in pipelines used for injection of seawater into oil fields. Appl. Environ. Microbiol. 74, 2841–2851. https://doi.org/10.1128/AEM.02027-07.

Shaffer, J.P., Carpenter, C.S., Martino, C., Salido, R.A., Minich, J.J., Bryant, M., Sanders, K., Schwartz, T., Humphrey, G., Swafford, A.D., Knight, R., 2022. A comparison of six DNA extraction protocols for 16S, ITS and shotgun metagenomic sequencing of microbial communities. Biotechniques 73, 34–46. https://doi.org/10.2144/btn-2022-0032.

Sharma, M., An, D., Liu, T., Pinnock, T., Cheng, F., Voordouw, G., 2017. Biocide-mediated corrosion of coiled tubing. PLoS One 12, e0181934. https://doi.org/10.1371/journal.pone.0181934.

Sharma, M., Menon, P., Voordouw, J., Shen, Y., Voordouw, G., 2018. Effect of long term application of tetrakis (hydroxymethyl) phosphonium sulfate (THPS) in a light oil-producing oilfield. Biofouling 34, 605–617. https://doi.org/10.1080/08927014.2018.1476500.

Shi, X., Zhang, R., Sand, W., Mathivanan, K., Zhang, Y., Wang, N., Duan, J., Hou, B., 2023. Comprehensive review on the use of biocides in microbiologically influenced corrosion. Microorganisms 11, 2194. https://doi.org/10.3390/microorganisms11092194.

Stoodley, P., deBeer, D., Lewandowski, Z., 1994. Liquid Flow in Biofilm Systems. Appl. Environ. Microbiol. 60 (8). https://doi.org/10.1128/aem.60.8.2711-2716.1994.

Videla, H.A., 2002. Prevention and control of biocorrosion. Int. Biodeterior. Biodegrad. 49, 259–270. https://doi.org/10.1016/S0964-8305(02)00053-7.

Wang, D., Kijkla, P., Mohamed, M.E., Saleh, M.A., Kumseranee, S., Punpruk, S., Gu, T., 2021. Aggressive corrosion of carbon steel by *Desulfovibrio ferrophilus* IS5 biofilm was further accelerated by riboflavin. Bioelectrochemistry 142, 107920. https://doi.org/10.1016/j.bioelechem.2021.107920.

Wang, D., Kijkla, P., Saleh, M.A., Kumseranee, S., Punpruk, S., Gu, T., 2022a. Tafel scan schemes for microbiologically influenced corrosion of carbon steel and stainless steel. J. Mater. Sci. Technol. 130, 193–197. https://doi.org/10.1016/j.jmst.2022.05.018.

Wang, D., Liu, J., Jia, R., Dou, W., Kumseranee, S., Punpruk, S., Li, X., Gu, T., 2020. Distinguishing two different microbiologically influenced corrosion (MIC) mechanisms using an electron mediator and hydrogen evolution detection. Corros. Sci. 177, 108993. https://doi.org/10.1016/j.corsci.2020.108993.

Wang, D., Yang, C., Saleh, M.A., Alotaibi, M.D., Mohamed, M.E., Xu, D., Gu, T., 2022b. Conductive magnetite nanoparticles considerably accelerated carbon steel corrosion by electroactive *Desulfovibrio vulgaris* biofilm. Corros. Sci. 205, 110440. https://doi.org/10.1016/j.corsci.2022.110440.

Wang, J., Liu, H., Mohamed, M.E.-S., Saleh, M.A., Gu, T., 2022. Mitigation of sulfate reducing *Desulfovibrio ferrophilus* microbiologically influenced corrosion of X80 using THPS biocide enhanced by Peptide A. J. Mater. Sci. Technol. 107, 43–51. https://doi.org/10.1016/j.jmst.2021.07.039.

Woodard, T.L., Ueki, T., Lovley, D.R., 2023. H_2 is a major intermediate in *Desulfovibrio vulgaris* corrosion of iron. mBio 14, e00076-23. https://doi.org/10.1128/mbio.00076-23.

Xu, D., Gu, T., Lovley, D.R., 2023. Microbially mediated metal corrosion. Nat. Rev. Microbiol. 21, 705–718. https://doi.org/10.1038/s41579-023-00920-3.

Xu, D., Li, Y., Song, F., Gu, T., 2013. Laboratory investigation of microbiologically influenced corrosion of C1018 carbon steel by nitrate reducing bacterium *Bacillus licheniformis*. Corros. Sci. 77, 385–390. https://doi.org/10.1016/j.corsci.2013.07.044.

Xu, L., Guan, F., Ma, Y., Zhang, R., Zhang, Y., Zhai, X., Dong, X., Wang, Y., Duan, J., Hou, B., 2022. Inadequate dosing of THPS treatment increases microbially influenced corrosion of pipeline steel by inducing biofilm growth of *Desulfovibrio hontreensis* SY-21. Bioelectrochemistry 145, 108048. https://doi.org/10.1016/j.bioelechem.2021.108048.

Xu, L., Khan, A., Aqeel, S.A., Alqahtani, A., AlSharif, L., Kijkla, P., Kumseranee, S., Punpruk, S., Gu, T., 2025a. Distinguishing abiotic corrosion from two types of microbiologically influenced corrosion (MIC) using a new electrochemical biofilm/MIC test kit. J. Environ. Manag. 374, 124093. https://doi.org/10.1016/j.jenvman.2025.124093.

Xu, L., Khan, A., Wang, D., Kijkla, P., Kumseranee, S., Punpruk, S., Aqeel, S.A., Gu, T., 2025b. Two-electrode electrochemical scans vs. three-electrode scans in microbiologically influenced corrosion detection with various counter electrode/pseudo-reference electrode materials. Bioelectrochemistry 165, 109002. https://doi.org/10.1016/j.bioelechem.2025.109002.

Xu, L., Kijkla, P., Kumseranee, S., Punpruk, S., Gu, T., 2024. "Corrosion-resistant" chromium steels for oil and gas pipelines can suffer from very severe pitting corrosion by a sulfate-reducing bacterium. J. Mater. Sci. Technol. 174, 23–29. https://doi.org/10.1016/j.jmst.2023.01.008.

Xu, R., Yu, Z., Zhang, S., Meng, F., 2019. Bacterial assembly in the bio-cake of membrane bioreactors: stochastic *vs.* deterministic processes. Water Res. 157, 535–545. https://doi.org/10.1016/j.watres.2019.03.093.

Yang, J., Wang, Z., Qiao, Y., Zheng, Y., 2022. Synergistic effects of deposits and sulfate reducing bacteria on the corrosion of carbon steel. Corros. Sci. 199, 110210. https://doi.org/10.1016/j.corsci.2022.110210.

Zhou, C., Vannela, R., Hayes, K.F., Rittmann, B.E., 2014. Effect of growth conditions on microbial activity and iron-sulfide production by *Desulfovibrio vulgaris*. J. Hazard Mater. 272, 28–35. https://doi.org/10.1016/j.jhazmat.2014.02.046.

Zuo, R., 2007. Biofilms: strategies for metal corrosion inhibition employing microorganisms. Appl. Microbiol. Biotechnol. 76, 1245–1253. https://doi.org/10.1007/s00253-007-1130-6.